Fabric Texture Analysis Using Computer Vision Techniques

Xin Wang, Nicolas D. Georganas, *Life Fellow, IEEE*, and Emil M. Petriu, *Fellow, IEEE*

***Abstract*—This paper presents inexpensive computer vision techniques allowing to measure the texture characteristics of woven fabric, such as weave repeat and yarn counts, and the surface roughness. First, we discuss the automatic recognition of weave pattern and the accurate measurement of yarn counts by analyzing fabric sample images. We propose a surface roughness indicator FD_{FFT}, which is the 3-D surface fractal dimension measurement calculated from the 2-D fast Fourier transform of high-resolution 3-D surface scan. The proposed weave pattern recognition method was validated by using computer-simulated woven samples and real woven fabric images. All weave patterns of the tested fabric samples were successfully recognized, and computed yarn counts were consistent with the manual counts. The rotation invariance and scale invariance of FD_{FFT} were validated with fractal Brownian images. Moreover, to evaluate the correctness of FD_{FFT}, we provide a method of calculating standard roughness parameters from the 3-D fabric surface. According to the test results, we demonstrated that FD_{FFT} is a fast and reliable parameter for fabric roughness measurement based on 3-D surface data.**

***Index Terms*—Computer vision, fractal dimension, fuzzy c-means clustering (FCM), grey level cooccurrence matrix (GLCM), principal component analysis (PCA), surface roughness, texture analysis, woven fabric.**

I. Introduction

THE PROCESS automation of textile and clothing manufacturing has been of increasing interest over the decades. This is still a challenging task because of the unpredictable variability of fabric material properties. There is a need for the development of more efficient computer techniques for the automated control of the fabric manufacturing process. In addition, due to the increasing demand of consumers for high-quality textile products, an automatic and objective evaluation of the fabric texture appearance is necessary with respect to geometric structure characteristics, surface and mechanical properties, and, not the least, aesthetic appearance. The accurate measurement of fabric texture parameters, such as weave structure, yarn counts, and surface roughness, has wide applications not only in the textile industry but also in other areas, such as virtual environments, e-commerce, and robotic telemanipulation.

Manuscript received December 14, 2009; revised March 1, 2010; accepted April 1, 2010. Date of publication September 7, 2010; date of current version December 8, 2010. The Associate Editor coordinating the review process for this paper was Dr. Augusto Sarti.

The authors are with the School of Information Technology and Engineering, University of Ottawa, Ottawa, ON K1N 6N5, Canada.

Color versions of one or more of the figures in this paper are available online at http://ieeexplore.ieee.org.

Digital Object Identifier 10.1109/TIM.2010.2069850

In today's textile industry, the evaluation of fabric texture properties still relies on manual operations with the help of microscopes, which are very tedious and time consuming. The subjective nature of this inspection procedure leads to serious variation in quality assessment; hence, there is a permanent interest in the development of more efficient and objective methods for the quality control of these fabric properties.

One of the earlier major breakthroughs in the development of an objective methodology for fabric quality control has been the Kawabata Evaluation Systems for Fabrics (KES-F) [1], which was introduced in the 1980s. Although the KES-F systems have received wide attention, their high price and complicated methods lead the researchers to continue looking for alternative simpler, faster, and more cost-effective methods for quality control of fabrics.

Developments in computer vision and 3-D laser imaging technologies led to an increased research effort in image texture analysis for a large variety of applications, such as surface roughness inspection in manufacturing [2]–[5], texture classification [6], [7], defect recognition for textile quality control [8], [9], medical image inspection [10], [11], shape recognition [12], and liquid depth measurement [13].

This paper will present inexpensive computer vision and image-processing techniques for the measurement of geometric texture characteristics of woven fabrics. In Section II, we propose a new method for the automatic recognition of the weave pattern and accurate measurement of yarn counts by analyzing 2-D fabric sample images. In Section III, we present a new fabric surface roughness measurement method from high-resolution 3-D surface scans using 2-D fast Fourier transform (2DFFT)-based fractals. We also proposed a method to evaluate the standard roughness parameters from 3-D fabric surface scans.

We used Matlab [14] to implement our proposed methods and evaluate the results, as shown in Section IV.

II. Geometric Structure Measurement

Woven fabrics are highly structured materials, having their appearance and handling and mechanical properties influenced by their geometric structure. They are formed by two sets of mutually perpendicular and interlaced yarns: "warp" and "weft." Warp refers to the long vertical yarns that are wrapped around the looms. Weft refers to the horizontal yarns that are woven through the warp yarns.

The weave pattern and the yarn count are two major geometric characteristics of woven fabrics. Weave pattern refers to the basic unit of weave that is periodically repeated throughout

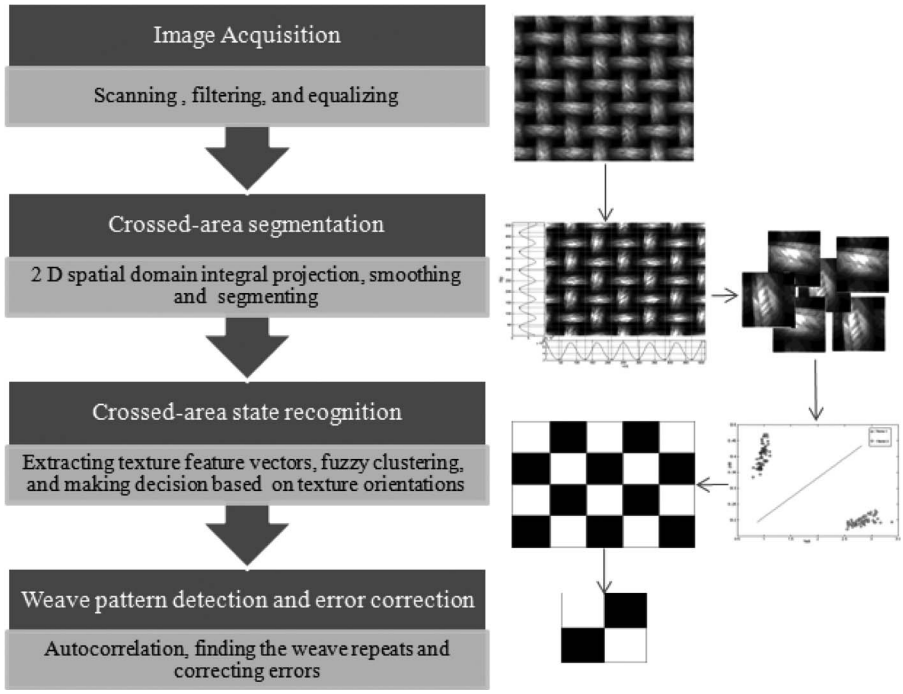

Fig. 1. Flowchart of automatic woven structure recognition.

the entire fabric area. Yarn count is defined as the number of yarns per centimeter. The weave pattern and the yarn count are characteristics that affect the dynamic behavior of the fabric. For example, different weave patterns have different effects on bending and shearing stiffness of fabric, and obviously, it leads to the different appearance of fabrics. Yarn count, as a measure of the fineness or coarseness of woven fabric, is also used as a measure of the fabric quality.

The automatic recognition of weave patterns has been reported by many researchers [15]–[24]. There are two main approaches. One approach is to extract global texture features either in spatial domain or frequency domain and then use a learning algorithm classifier to recognize weave pattern types [15], [17], [18], [21], [23], [24]. This approach is very sensitive to the selection of the set of training data used for the learning algorithm. Variations in the lighting condition and the image scale may lead to a failure of the classifier. Moreover, once a weave pattern is erroneously recognized by the classifier, it cannot be corrected. The second approach consists of two steps: 1) the detection of the crossed area of weft and warp yarns and 2) the detection of the crossed-area states, i.e., whether the weft or the warp floats over the other in this area. To detect the crossed area, one can use either 2DFFT [19], [20] or a 2-D autocorrelation in the spatial domain [22] to find the widths of weft and warp. As the widths of the yarns are not constants for real fabric samples, errors may occur when locating the crossed area of unevenly distributed yarns.

C. Kuo *et al.* [16] developed an unsupervised automatic recognition method in the spatial domain by using of fuzzy c-means clustering (FCM). Their method can identify several woven fabrics that have different yarn densities and various geometric shapes for the crossed area of yarns. As there are only two possible crossed-area states in which the weft or the warp is interlaced over the other, they used FCM to classify the detected crossed areas into two clusters. However, their method failed to decide whether the weft or the warp floats in a specific crossed area.

We presented a novel method for resolving the foregoing issues to recognize the accurate structure of woven fabric in [25]. By using 2-D integral projection to segment crossed areas of yarns, we can detect the crossed area of unevenly distributed yarns. We apply FCM to multiscale texture features based on the Grey level occurrence matrix to classify the different crossed-area states. The texture orientation features are calculated to determine the exact state of the crossed area. This paper reports further development, enhancing the performance of the recognition algorithm described in [25]. We use principal component analysis (PCA) to improve the classifier performance. An error correction method has been added to correct the detection errors in some crossed areas. We increase the yarn count accuracy by using 2-D integral projection.

A. Weave Pattern Recognition

The major steps for automatic weave structure recognition are shown in Fig. 1.

1) Preprocessing: To evaluate the proposed method, we use a number of computer-simulated woven material images and a number of fabric images extracted from different real woven fabrics. These images have different weave types, fiber appearances, and yarn counts. Simulated woven samples are generated in Filter Forge by applying programmable image-processing filters. The real fabric images are scanned using an HP scanner (Scanjet 4570c) with a resolution of 2400 dpi. For real fabric scan, it is very important to arrange the warp and the weft yarns properly along the x- and y-directions to achieve best performance for the crossed-area detection. Then,

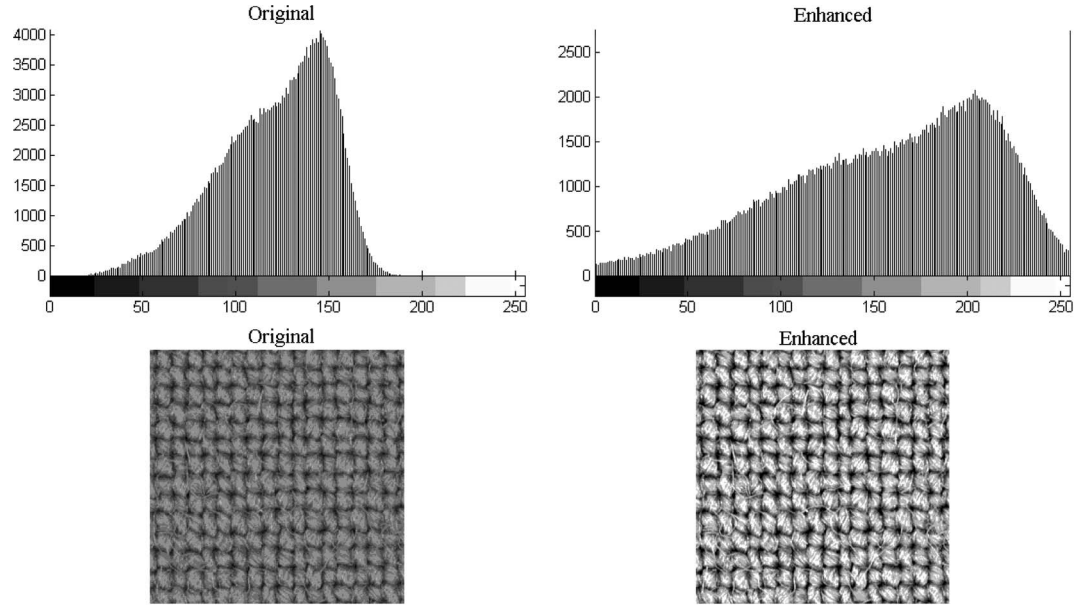

Fig. 2. Comparison between original and enhanced fabric images.

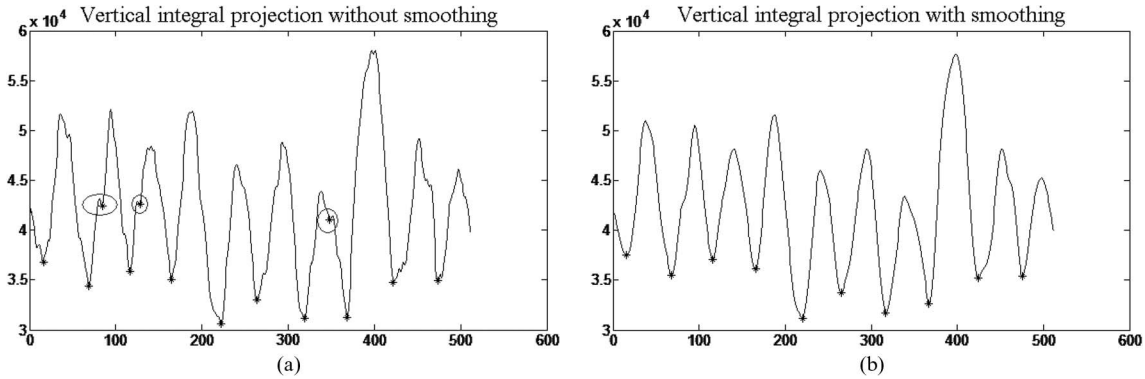

Fig. 3. Integral projections. (a) Original projection curve. (b) Projection curve after smoothing.

the images are resized into 600×600 pixels and then converted into grayscale for increasing the processing speed.

We use a frequency-domain Butterworth low-pass filter for reducing the noise. We employ the exponential function for histogram equalization for further image enhancement. Fig. 2 shows the results of image enhancement.

2) Crossed-Area Detection: To detect the interlacing area where weft yarn and warp yarn are crossed over each other, we apply a spatial-domain integral projection approach. Interstices between yarns display darkness; therefore, the pixels around them have relative lower grey levels. Looking for the local minima of the horizontal and vertical integral projections, we can locate the positions of interstices among yarns. Suppose $I(x, y)$ is an $M \times N$ grayscale image. The horizontal and vertical projection of the entire image is defined, respectively, as $H(y)$ and $V(x)$; thus, we have

$$H(y) = \sum_{x=1}^{N} I(x, y) \tag{1}$$

$$V(x) = \sum_{y=1}^{M} I(x, y). \tag{2}$$

Due to image complexity and noise, there are some small weaves throughout the projection curve, which interfere with actual local minima location detections. Therefore, we use a moving average filter to smooth the curves. The enhancement of smoothing is shown in Fig. 3. The left panel depicts an integral projection curve without smoothing. Undesired local minima, which are highlighted by a circle, are removed after smoothing (shown in the right panel).

Fig. 4 illustrates the relation between a woven fabric sample and its integral projections. The interstices between yarns exhibit the local lowest values. By finding the local minima of horizontal and vertical integral projections, the warp separation lines and weft separation lines are found, respectively. The crossed areas are identified by intersecting the warp separation lines with weft separation lines.

3) Crossed-Area State Recognition: Once we detect the crossed areas of the weft and warp yarns, we segment the fabric image into small image cells, which express the detected crossed areas. To determine the state of a crossed area, we have to analyze its texture features.

Multiscale and direction invariant texture feature extraction based on GLCM: The texture of an image is represented

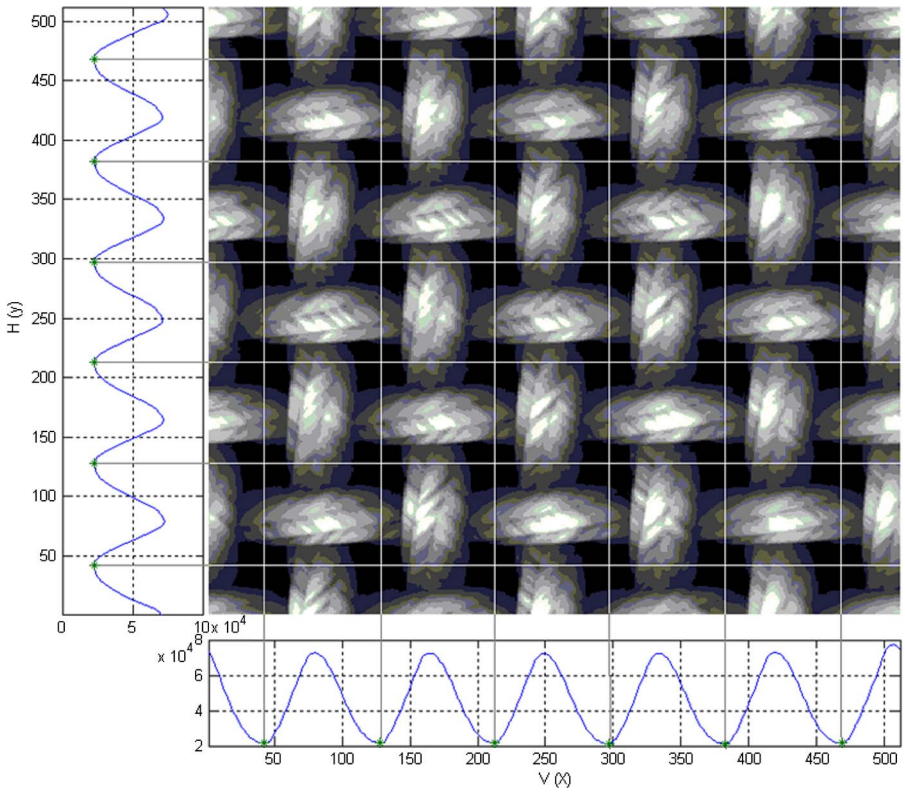

Fig. 4. Crossed-area detection.

TABLE I
DIRECTION VALUES

θ	0°	45°	90°	135°
θ_0	0	1	1	1
θ_1	1	1	0	-1

by the change of image gray levels. The grey level cooccurrence matrix (GLCM) of an image shows the statistic characteristics of gray level or gray level gradient under the condition of a certain spatial position. The features extracted from GLCM are related to the density of fiber and the orientation of yarn on a crossed area. We use GLCM-based texture features to discriminate the different crossed-area states.

GLCM is computed based on two parameters, which are the distance between the pixel pair d and their angular relation θ. θ is quantized in four directions (0°, 45°, 90°, and 135°). For rectangular $M \times N$ image segment $I(x, y)$, gray levels i and j, the nonnormalized GLCM P_{ij}'s are defined by

$$P_{ij}(\theta, d) = \sum_{x=1}^{N} \sum_{y=1}^{M} C\{(I(x, y) = i) \wedge (I(x \pm d\theta_0, y \mp d\theta_1) = j)\} \quad (3)$$

where $C\{.\} = 1$ if the argument is true and $C\{.\} = 0$ otherwise. The $\pm$ and $\mp$ signs in (3) mean that each pixel pair is counted twice: once forward and once backward to make the GLCM diagonal symmetric. For each direction, θ_0 and θ_1 are shown in Table I.

We calculate eight GLCM texture features, which are studied by Haralick [26]: 1) contrast (CON); 2) dissimilarity (DIS); 3) homogeneity (HOM or inverse difference moment); 4) angular second moment (ASM); 5) entropy (ENT); 6) GLCM mean (μ_i, μ_j); 7) variance (VAR : σ_i^2, σ_j^2); and 8) correlation (COR).

The width of yarns varies from sample to sample. The orientations of fibers that form the yarn also change over the detected crossed areas. To reduce the recognition errors caused by the preceding issues, we calculate the foregoing eight texture features with multiple distance $d = 1, 2, 4, 6, 8, 10$ pixels and four angular directions. Thus, for each detected crossed area, we have $8 \times 6 \times 4 = 192$ texture features. A feature vector of detected crossed area is formed by these 192 values.

Principal component analysis: A feature vector has 192 elements. By definition [26], the GLCM features are interrelated. Moreover, the diversity of the fabric samples also makes the measured feature vectors become confusing. The measured feature vector sets appear clouded and may be redundant. This obstructs the accuracy of the next classification. As a standard tool in modern data analysis, PCA applies to large areas from image processing to bioscience. The goal of PCA is to extract relevant information from data sets consisting of a large number of interrelated variables [27]. Therefore, PCA is the optimal method to solve the preceding problems. We can state that our goals for using PCA are 1) to minimize redundancy in our feature vector sets and 2) to maximize the signal that was expressed by our feature vectors.

The basic idea of PCA is to identify the most meaningful basis to reexpress the data set. In our studies, we assume that each fabric image has m-detected crossed areas, and each crossed area is expressed by a feature vector with 192 elements.

The feature data set for a fabric image is a $192 \times m$ matrix X. By using PCA, we aim at finding a new basis B that will reveal an optimal representation Y of the original data set X. The row vectors of B will become the principal components of X. Geometrically, B is a linear transform that rotates and stretches X into Y, i.e.,

$$BX = Y. \tag{4}$$

The basic steps for determining B in our studies are the following:

Step 1: Calculate the mean of each dimension as

$$\overline{x}_i = \sum_{j=1}^{m} x_{ij}. \tag{5}$$

Step 2: Subtract off the mean for each dimension to produce a zero mean data set $\widetilde{X}$.

Step 3: Construct the matrix Y, where $Y = \widetilde{X}^T/\sqrt{m-1}$.

Step 4: Compute the singular value decomposition (SVD) [28] of matrix Y. SVD produces a diagonal matrix S with nonnegative diagonal elements in decreasing order and unitary matrices U and V so that $Y = USV^T$. The column vectors v_i of V are the principal components.

Step 5: Choose the first k principal components v_i by using the following criterion:

$$\frac{\sum_{i=1}^{k} \lambda_i}{\sum_{i=1}^{n} \lambda_i} > Threshold \tag{6}$$

where λ_i represents the main diagonal elements of S. m is the number of dimensions in our case 192. We choose the threshold as 0.95. Thus, a new linear transform B is formed by $B = [v_1 \quad v_2 \quad \cdots \quad v_k]^T$.

Step 6: Project the data set $\widetilde{X}$ to an optimized feature vector set Y by applying (4).

The first benefit of the PCA method is dimension reduction. The dimension of our new feature data set Y is no longer 192 but $k \ll 192$. According to our experimental results, k varies over the range from 1 to 17 for different fabric samples. k tends to be larger when the hairiness and orientation of fibers in crossed areas are messier. The average size of k is around 6. The other primary motivation behind this method is to decorrelate the original data to remove second-order dependencies for accurate classification in the next step.

FCM: We use FCM [29] to classify the two possible different crossed-area states. FCM is based on minimizing the following objective function for the partition of data set $X = \{x_1, x_2, \ldots, x_n\}$ given by:

$$J_m = \sum_{i=1}^{c} \sum_{k=1}^{n} u_{i,k}^m \|x_k - v_i\|^2. \tag{7}$$

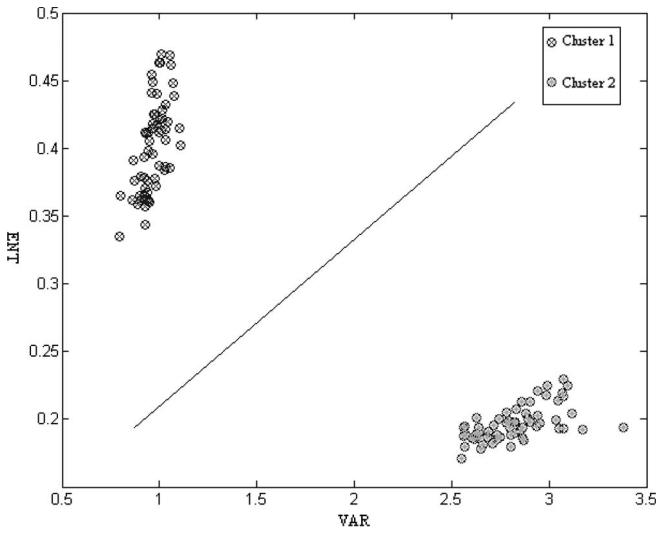

Fig. 5. Example of FCM clustering.

In (7), n is the number of data vectors, c is the number of clusters with $1 < c \leq n$, $u_{i,k}$ is the degree of membership of x_k in the ith cluster, m $(1 < m < \infty)$ is a weighting exponent that influences the fuzziness of the membership function, and v_i is the center of the ith cluster. The norm $\|x_k - v_i\|$ is the distance between the sample x_k and the centers of classes v_i.

In our studies, we want to classify a set of texture feature vectors with k dimensions into two clusters. The algorithm can be summarized by the following steps:

Step 1: Initialization (iteration 0)

Scan the yarn crossed areas through the whole sample image to construct the data set X containing the feature vectors of each crossed-area segments.

Set $c = 2$ and $m = 1.5$.

Randomly choose the centers of clusters v_i.

From the iteration $t = 1$ to the end of the algorithm:

Step 2: Compute the membership function $u_{i,k}$ using:

If $\|x_k - v_i\| = 0$, then set $u_{i,k} = 1$ and $u_{i,k} = 0$ (for $i \neq k$).

If $\|x_k - v_i\| \neq 0$, then

$$u_{i,k} = \left(\sum_{j=1}^{c} \left(\frac{\|x_k - v_i\|}{\|x_k - v_j\|} \right)^{2/m-1} \right)^{-1}. \tag{8}$$

Step 3: Update the positions of the centers v_i using

$$v_i = \frac{\sum_{k=1}^{n} u_{i,k}^m x_k}{\sum_{k=1}^{n} u_{i,k}^m}. \tag{9}$$

Step 4: Termination test: If $\|U^{(t+1)} - U^{(t)}\| > \varepsilon$, then increment the iteration t, and back to Step 2; otherwise, stop the algorithm. ε is the termination criterion.

Since the feature data set has more than three dimensions, the results of classification cannot be shown in a single diagram. Fig. 5 illustrates the clustering of FCM by the two texture features (ENT and VAR) for a fabric sample.

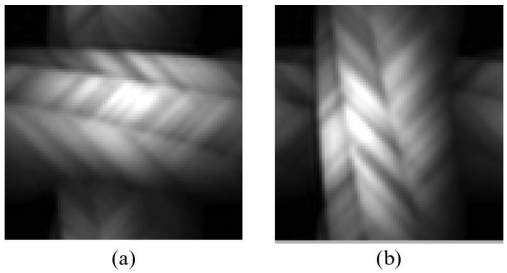

Fig. 6. Detected crossed areas. (a) Weft float. (b) Warp float.

Once we find two clusters of crossed-area segments, we have to determine their exact states in which the warp is interlaced over the weft or vice versa. Since the woven fabric is made only by interlacing the warp yarns in the vertical direction and the weft yarns in the horizontal direction, the orientations of the texture in detected segments are different depending on the type of the float yarn, as shown in Fig. 6. By analyzing the texture orientation features of the clusters, we can recognize their actual states.

We compute average "covariabilities" [30] as the texture orientation features to determine the state of the crossed area. These features show gray-level average difference between two pixels according to their distance d and orientation. Horizontal and vertical covariabilities in a detected segment $I(x, y)$ with size $M \times N$ are calculated as follows:

$$COV\_H(d) = \frac{1}{M \times (N-d)} \times \sum_{y=1}^{M} \sum_{x=1}^{N-d} |I(x,y) - I(x+d,y)| \quad (10)$$

$$COV\_V(d) = \frac{1}{N \times (M-d)} \times \sum_{x=1}^{N} \sum_{y=1}^{M-d} |I(x,y) - I(x,y+d)| . \quad (11)$$

We compute the average horizontal and vertical covariabilities of each classified cluster. A fuzzy-rule-based decision is made for each cluster. The cluster with higher horizontal covariabilities and lower vertical covariabilities is determined as weft float, namely, the weft yarn is crossed over the warp yarn, and the other cluster is warp float.

4) Weave Pattern Detection and Error Correction: We use 0s and 1s to denote two different crossed-area states, i.e., the weft float and the warp float, respectively. For a fabric sample, a matrix C, which represents the detected crossed-area states, is formed with 0s and 1s. We assume that the fabric sample has M warp yarns and N weft yarns. Thus, there are $M \times N$ crossed areas detected in the fabric sample, and the size of C is $M \times N$. Let matrix W denote the basic unit of weave, i.e., weave pattern. Thus, C can be formed by tiling the basic unit matrix W periodically. The size of W can be found from the 2-D autocorrelation of C by finding the fundamental periods in weft and warp directions. The autocorrelation matrix R is computed as follows:

$$R(i,j) = \sum_{m=1}^{M} \sum_{n=1}^{N} C(m,n)C(m+i,n+j) \quad i = 1, \ldots, 2M-1; \quad j = 1, \ldots, 2N-1. \quad (12)$$

The fundamental period in warp direction (n_0) is determined by the integer distance from the center element $R(M, N)$ to the nearest peak in the Nth column. Similarly, the fundamental period in the weft direction (m_0) is the integer distance from $R(M, N)$ to the nearest peak in the Mth row. The size of W is $m_0 \times n_0$. To determine W, we cut an $m_0 \times n_0$ tile W' from C randomly. A matrix C' is formed by repetitively titling W'. In most cases, there are detection errors in C; the selected W' may have error as well. C', as an estimate of C, may have a number of different elements from C. The detection error of the fabric sample is computed by counting these different elements. We assume that the majority of the crossed-area states are detected correctly. Therefore, the tile W' with the lowest value of detection error is chosen as the basic weave pattern. The corresponding C' represents the correct detected crossed-area states.

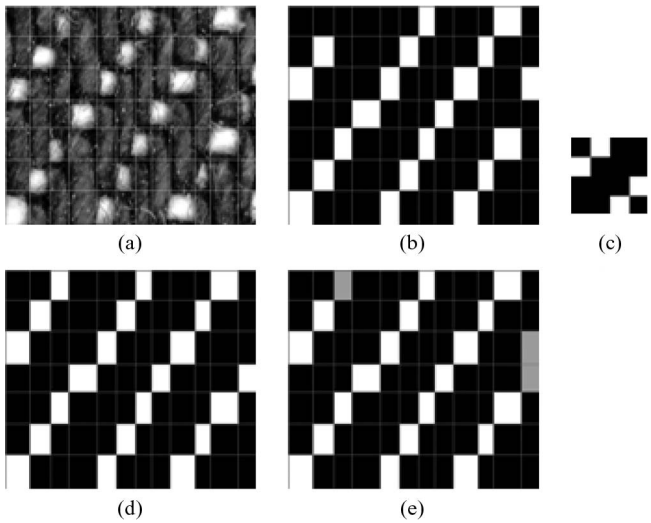

Fig. 7. Example of weave pattern detection and error correction. (a) A fabric sample. (b) The detected crossed-area states. (c) The basic weave pattern. (d) The estimation of crossed-area states. (e) The detected error.

Fig. 7 illustrates an example of weave pattern detection and error correction. A fabric sample is shown in (a). The black blocks and the white blocks represent the warp float and the weft float, respectively. The detected crossed-area states without error correction are shown in (b). The basic weave pattern is identified in (c). After the error-correction process, three errors, which are denoted by grey blocks, are detected as shown in (e). The detection errors occur in the classification step. Figure (d) illustrates the correct crossed-area states.

B. Automatic Measurement of Yarn Count

Vision-based image analysis has been used to monitor yarn density and yarn counts in many papers. For example,

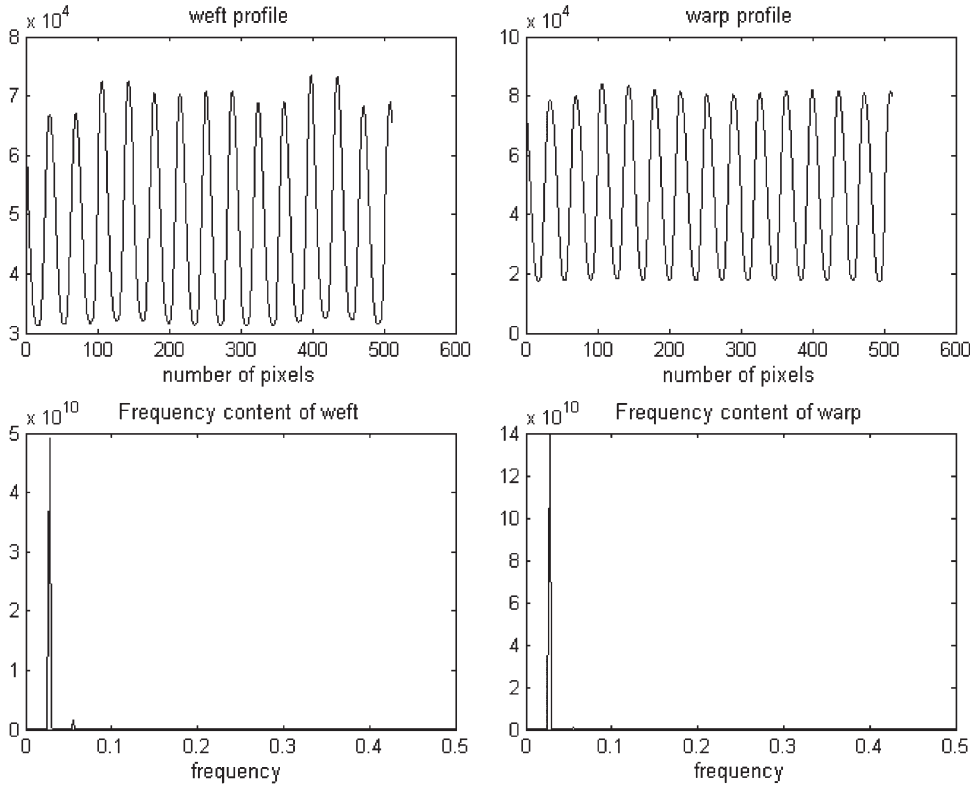

Fig. 8. Example of weft and warp profiles and their power spectra.

Sari-Sarraf and Goddard [31] determined the yarn density by analyzing the power spectrum of fabric images. However, the power spectrum of the original fabric image is too noisy to analyze in most cases. Instead of applying fast Fourier transform (FFT) to the entire original fabric image, we take advantage of horizontal and vertical projections, i.e., $H(y)$ and $V(x)$, which are computed in Section I. We consider $H(y)$ and $V(x)$ as the weft profile and the warp profile, respectively. Yarn counts are determined from the 1-D FFT of the profiles. In power spectrum, an overwhelming spike next to the zero depicts the individual share of the width of a yarn. The reciprocal of the distance from the spike to the origin is the estimate of the yarn count. Fig. 8 illustrates a weft profile, a warp profile of a plain weave sample, and their power spectra.

III. Surface Roughness Measurement

Surface roughness is a very important property of fabric in terms of both physical quality and aesthetic aspect. The KES-F system has an instrument specifically designed for evaluating fabric surface roughness. It measures the height variation of a fabric surface over a certain length along the weft and warp directions by using a stylus-based equipment. However, the force, which is imposed when measuring, actually affects the accuracy of the roughness measurement. Moreover, the roughness profile obtained from the KES tester is just 2-D. Three-dimensional surface roughness data can only be acquired by doing multiple scans of the fabric surface. It is slow and needs a complicated operation of the instrument. Therefore, the trend to use the noncontact method of surface roughness assessment on the 3-D surface data is inevitable and beneficial.

In recent years, along with the revolution of computer vision and image-processing technology, numerous methods for noncontact surface roughness assessment were proposed by scientists. For example, Gunarathne [5] introduced the specular reflection coefficient as a surface roughness measure by using an ultrasonic spectroscopy technique. Optical fiber sensors had been employed to accurately measure surface roughness in [3] and [4]. Moslehpour *et al.* [2] developed a portable surface roughness inspection probe to optically evaluate surface finish quantitatively. From their work, it can be concluded that a noncontact surface roughness measurement is faster than the traditional stylus-based method with high accuracy and is particularly nondestructive.

Fractal dimension is a parameter frequently used to analyze surface roughness. There are several alternative definitions of the fractal dimension, and consequently, many algorithms have been proposed to determine its value. For example, Kang *et al.* [32] use wavelet-based fractal dimension measurement to evaluate the surface roughness of wrinkle replicas and seam pucker samples. The estimation of fractal dimension is computed by applying linear regression on the averages of absolute wavelet coefficients in horizontal and vertical directions with respect to the decomposition levels. Although their measurement is claimed to be scale invariant, it actually is not robust to image rotations because only two direction data are studied. In our previous study [33], we found that the fractal dimension measurement based on 2DFFT analysis of fabric images is a scale-invariant and rotation-invariant parameter to evaluate the surface roughness of fabrics. In this paper, we extend our 2DFFT-based fractal method to 3-D surface data, which are obtained from high-resolution 3-D laser scanning. The

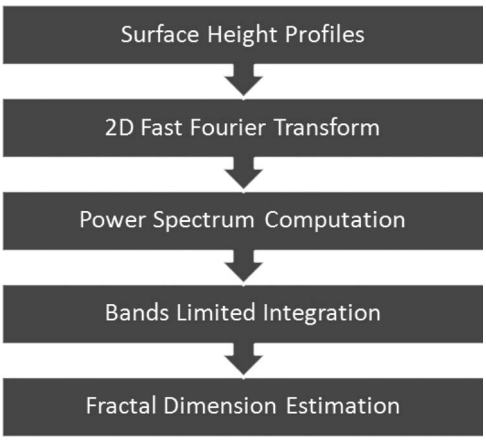

Fig. 9. General steps of the fractal dimension estimation by using 2DFFT power spectrum integration.

calculation of standard roughness parameters using these 3-D scans is also introduced as a supplementary reference to evaluate our method.

A. Estimation of Fractal Dimension

As shown in [34], the power spectrum $P(\omega)$ is proportional to the certain power β of the radial frequency ω, i.e.,

$$P(\omega) \propto \omega^{-\beta} \tag{13}$$

where $\beta \geq 0$. The fractal dimension (FD) of an image is related to the exponent β in (13), i.e.,

$$FD_{\mathrm{FFT}} = \frac{8-\beta}{2} \tag{14}$$

where FD_{FFT} denotes our fractal dimension estimate based on 2DFFT.

The general algorithm of our fractal dimension estimation is shown in Fig. 9. Fabric samples are cut into 5 × 5 cm pieces. Three-dimensional points of the fabric surface are gathered from 3-D laser scanning with very high resolution up to 1 μm. The raw 3-D data consist of a large number of 3-D coordinates with range from 281 880 to 523 308 points/fabric sample. Thus, there are around 11 230 to 20 930 points/cm^2/square centimeter. Originally, these points are not uniformly distributed over the 3-D space; therefore, it is too difficult to apply a data-processing algorithm. To simplify the problem, we use triangular linear interpolation to estimate fabric surface profiles on a uniformly spaced rectangular 2-D grid. The reconstructed surface profiles are stored into matrices. By applying the 2DFFT, the information is transformed to the spatial frequency domain. The power spectrum is calculated to remove the imaginary part of the 2DFFT result. We want to make a rotation-invariant measurement. For this purpose, the power spectrum is cut into 24 radial slices and integrated, respectively. The final step consists of determining the exponent β by using linear regression to find the slopes of the fourth step results on a log–log scale and applying (14) to compute FD_{FFT}. According to the properties of Fourier transform, theoretically, this measurement is robust to linear translations and scaling as well. The results of our robust test shown in Section IV also prove its good performance.

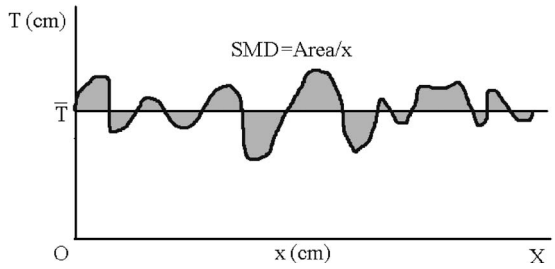

Fig. 10. Definition of geometrical roughness (SMD).

B. Estimation of Standard Surface Roughness Parameters

The geometrical roughness in the KES system is described as follows and shown in Fig. 10, where T represents the thickness of the fabric sample, and $\overline{T}$ denotes the average of T:

$$\mathrm{SMD} = \frac{1}{X}\int_0^X |T-\overline{T}|dx. \tag{15}$$

In practical terms, another standard roughness parameter is the root mean square (RMS) given by

$$\mathrm{RMS} = \sqrt{\frac{1}{X}\int_0^X |T-\overline{T}|^2 dx}. \tag{16}$$

A reference surface, which has minimum-distance values at all points of the fabric surface scan, is taken as global surface from which SMD and RMS are calculated. The surface profile is obtained from the 3-D fabric surface scan on an $N \times N$ mesh grid. We determine the reference surface $z = f(x,y) + \varepsilon$ for every fabric surface profile by applying a least-square method to minimize ε. We modify (15) and (16) to fit our 3-D cases as follows:

$$\mathrm{SMD}_i = \frac{1}{N^2}\sum_{m=1}^{N}\sum_{n=1}^{N} d_{m,n}^i$$

$$\mathrm{RMS}_i = \sqrt{\frac{1}{N^2}\sum_{m=1}^{N}\sum_{n=1}^{N}\left(d_{m,n}^i\right)^2} \tag{17}$$

where N is the number of mesh points along each direction, and $d_{m,n}^i$ is the minimum distance from the point of the 3-D surface profile at the mth row and nth column to the reference surface. The simplest reference surface is the flat plane $z = a_0 + a_1 x + a_2 y$, and the $d_{m,n}^i$ can be computed by

$$d_{m,n}^i = \frac{|a_0 + a_1 x_n + a_2 y_m - h_i(x_n, y_m)|}{\sqrt{a_1^2 + a_2^2 + 1}}. \tag{18}$$

We also consider the second-order polynomial surface $z = a_0 + a_1 x + a_2 y + a_3 x^2 + a_4 xy + a_5 y^2$ as an alternative reference surface. Fig. 11 shows an example of the relation between the reference surfaces and the actual fabric surface points. It is

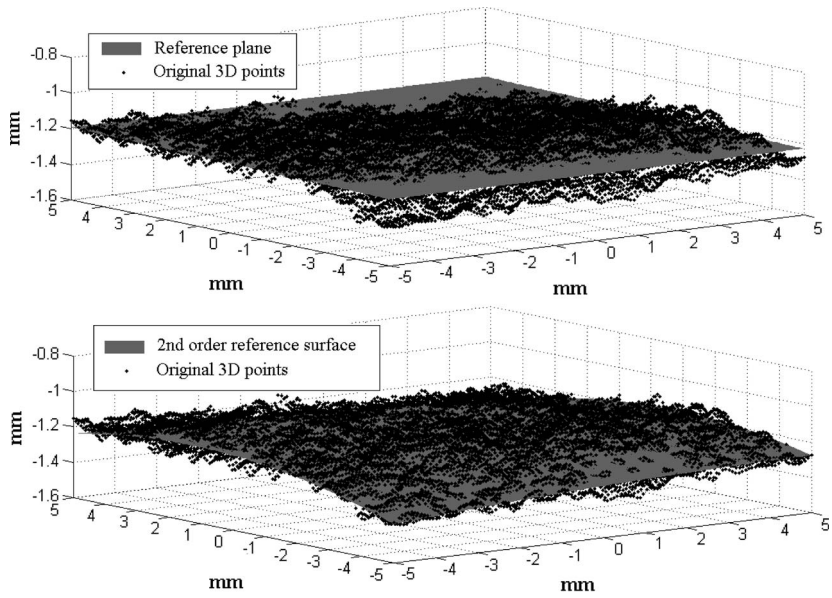

Fig. 11. Example of the reference surfaces with respect to surface points.

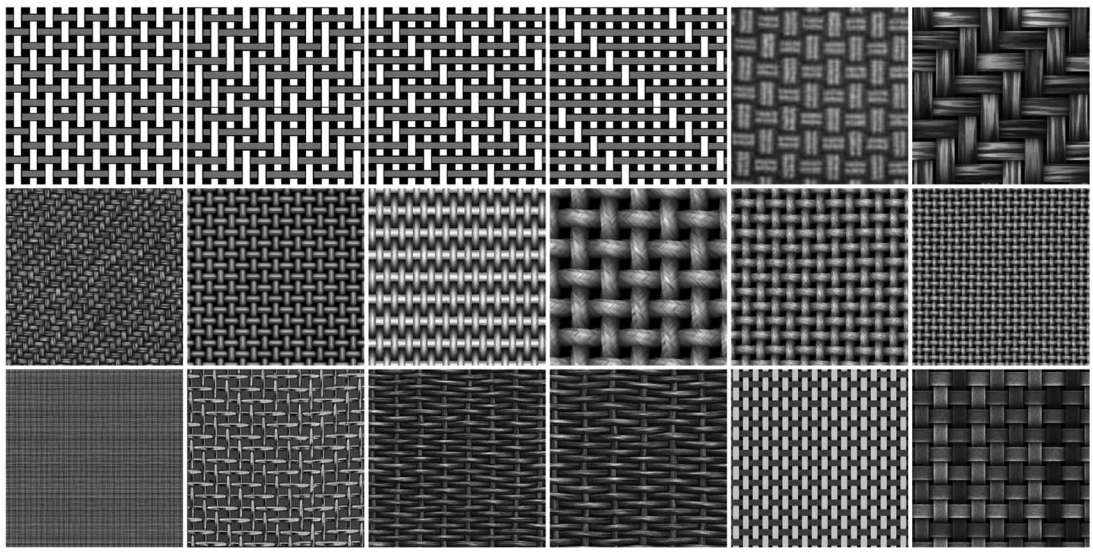

Fig. 12. Part of computer-simulated samples used in weave structure recognition.

obvious that the second-order polynomial surface fits the points better than the flat plane. However, a tradeoff has to be made between computation time and accuracy.

IV. Experiments and Results

A. Structure Measurement Experiment

To evaluate the proposed method, both computer-simulated samples and real woven fabric images were used. These images have different weave types, fiber appearances, and yarn counts. Fig. 12 shows part of the computer-simulated woven material images, and Fig. 13 shows the real fabric samples that we used. The recognition rate for the computer-simulated images is 100% before the error correction module. The error rate for real fabric samples is shown in Table II. The error may be caused by a local defect of the fabric surface, the low quality of the fabric image, or a bad segmentation. Since more than 95% crossed-area states are correctly detected, the result conforms to the assumption we made for our error correction algorithm. The recognition rates increased to 100% after error correction.

From the obtained results, we can conclude that with the proposed method for automatic weave structure recognition, all actual weave structures are well detected in different samples, which have different weave types, yarn appearances, and yarn counts. The yarn counts were repetitively computed five times with different segments of the same fabric sample. The results are shown in Fig. 14. The high consistency with the manual measurements shows the validity of our method. The low average variance demonstrates the reliability of our method. The test variance tends to be higher when the variance of the yarn width or the variance of yarn distribution is larger. The manual counts are slightly higher than the computer-determined yarn count because we round up the decimal numbers of yarn to integers during the manual count.

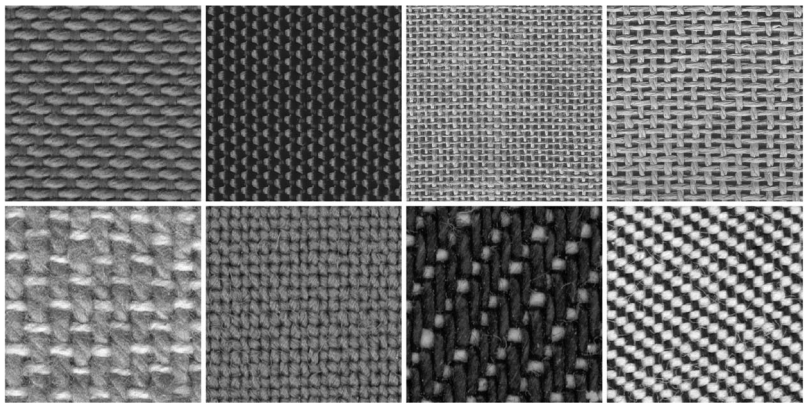

Fig. 13. Real woven fabric samples used in weave structure recognition.

TABLE II
DETECTION ERROR RATE FOR REAL FABRIC SAMPLES

Sample	P1	P2	P3	P4	P5	P6	T1	T2	Average
Error rate	0.029	0	0.044	0.035	0.028	0.029	0.036	0.018	0.027

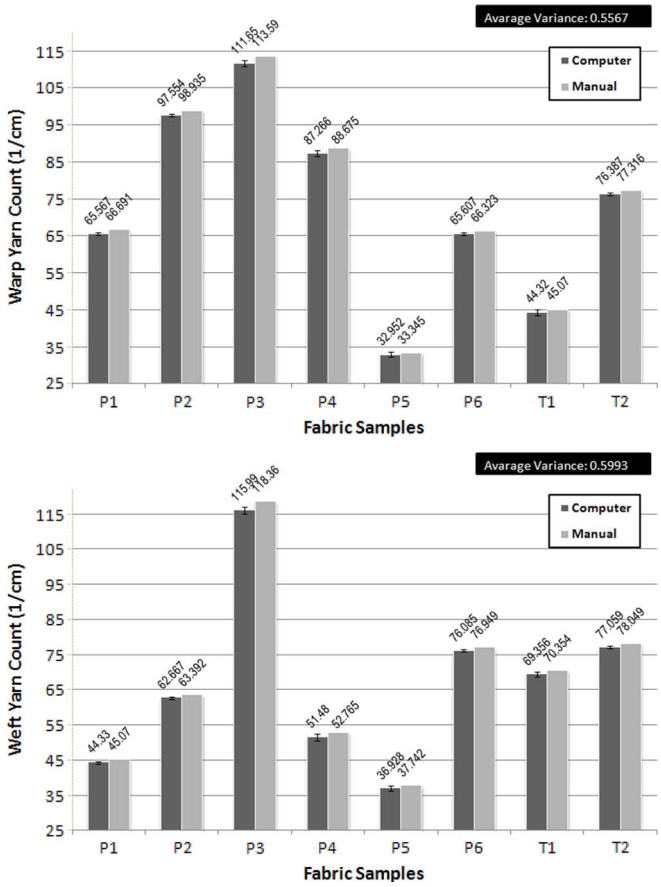

Fig. 14. Yarn counts for real fabric samples. p1–p6: plain weave samples. t1–t2: twill weave samples.

B. Surface Roughness Measurement Experiment

To demonstrate the robustness of our fractal dimension measurement FD_{FFT}, we used computer-simulated fractal Brownian surfaces, as shown in Fig. 15. Two simulation algorithms were used: one is the fractal Brownian motion interpolation, and the other is the random midpoint displacement (RMDs). The original size of the test images is 256 $\times$ 256 pixels. For testing the effects of scaling, we magnified the simulated fractal images into 512 $\times$ 512 pixels. The computed FD_{FFT}s compared with the theoretical fractal dimension are shown in Table III. Pearson's correlation coefficients were computed between theoretical values and each group of FD_{FFT}s as well. The computed correlation coefficients are all greater than 0.978. It shows that FD_{FFT}s are highly correlated with the theoretical ones. For testing the effects of rotations, we rotated the images in counterclockwise direction by an angle every 15° from $-90°$ to 90°. The nearest-neighbor interpolation was used for image rotation. Table IV lists the average values of FD_{FFT}s measured from image rotations and the corresponding measurement variance. Due to the smoothing effect of interpolation, the FD_{FFT} measurement after angular rotation is slightly lower than that of the previous test. The variance of the measurements for multiple angular rotations is on the order of 10^{-3}, and it proves that our measurement is robust to rotation.

To validate the goodness of FD_{FFT} as a parameter for evaluating fabric surface roughness, ten 3-D fabric surface scans were cut into square pieces of size 1 cm^2 and converted into surface profiles based on 256 $\times$ 256, 128 $\times$ 128, 64 $\times$ 64 mesh grids, respectively. To investigate the effects of the conversion from the unevenly distributed 3-D points to the uniformly distributed mesh points, we compared the mean and variance of the original points to those of the corresponding mesh points. The results are shown in Fig. 16. The values of mean and variance are quite close to each other. It shows that the original surface points and the corresponding mesh surface points represent the same surface under high probabilities. Fig. 17 illustrates a comparison between the original surface points and the reconstructed surface on a 64 $\times$ 64 mesh grid. Although the number of surface points has been reduced to 64^2, most of the original surface points still sit on the reconstructed surface. Therefore, the noise introduced by the triangular interpolation can be neglected.

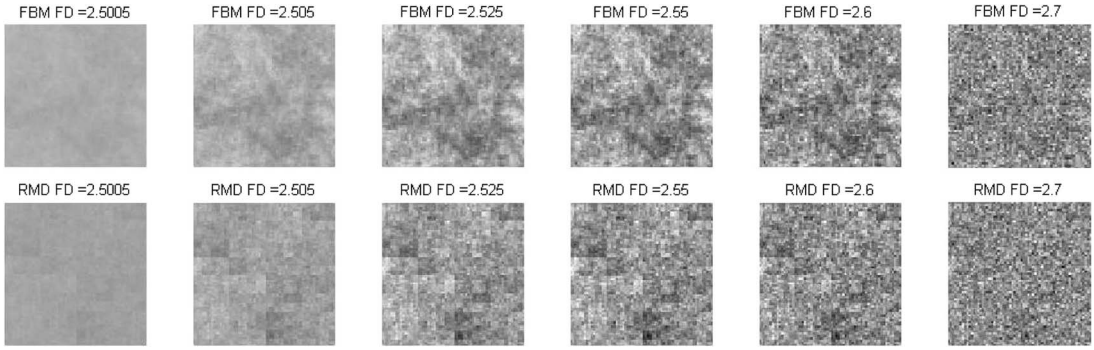

Fig. 15. Computer-simulated 2-D fractal Brownian motion images with different theoretical fractal dimension.

TABLE III
FRACTAL DIMENSION MEASUREMENTS ON COMPUTER-SIMULATED FRACTAL BROWNIAN SURFACES

Theoretical FD	FBMs	FBMs (×2)	RMDs	RMDs (×2)
2.5005	2.4512	2.5964	2.4546	2.5858
2.5050	2.4515	2.5988	2.4524	2.5909
2.5250	2.4906	2.6338	2.4887	2.6247
2.5500	2.5383	2.6733	2.5348	2.6636
2.6000	2.6407	2.7735	2.6358	2.7639
2.7000	2.8554	2.9288	2.8476	2.9170
Correlation Coefficient	0.9993	0.9789	0.9903	0.9784

TABLE IV
FRACTAL DIMENSION MEASUREMENTS ON FRACTAL BROWNIAN SURFACES WITH MULTIPLE ANGULAR ROTATIONS

Theoretical FD	FBMs (Average μ)	FBMs (Variance σ^2)	RMDs (Average μ)	RMDs (Variance σ^2)
2.5005	2.3818	0.0023136	2.3971	0.0021236
2.5050	2.4204	0.0018512	2.4630	0.0010234
2.5250	2.5052	0.0013555	2.5488	0.0007033
2.5500	2.5511	0.0010023	2.5962	0.0006849
2.6000	2.6058	0.0005921	2.6543	0.0007527
2.7000	2.6994	0.0013178	2.7147	0.0013980

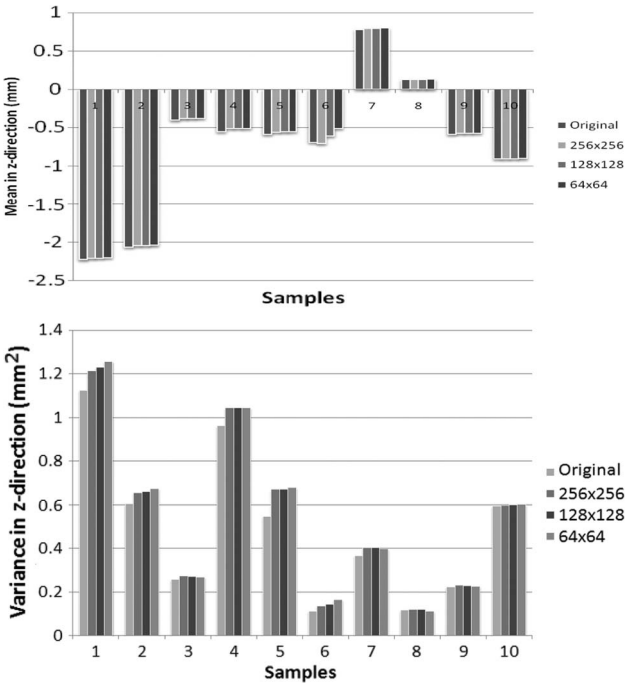

Fig. 16. Comparison of the original 3-D data points and the reconstructed surface points after interpolation.

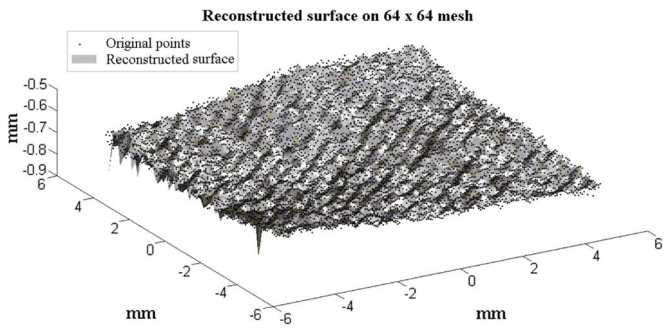

Fig. 17. Example of the original 3-D surface points versus the reconstructed surface based on a rectangular 64 × 64 mesh grid.

Both standard roughness parameters and FD_{FFT}s were computed to examine the relationship between FD_{FFT} and the standard roughness parameters. The FD_{FFT} measurements are plotted with respect to the standard roughness parameters, as shown in Fig. 18. The computation times of FD_{FFT}, SMD, and RMS are shown in Fig. 19. The FD_{FFT} calculated from mesh data consistently decrease as the SMD and RMS increase. The Pearson's correlation coefficients between the FD_{FFT}s of the 256 × 256 and 128 × 128 mesh grids and the corresponding SMDs and RMSs are greater than 0.93. For the 64 × 64 mesh

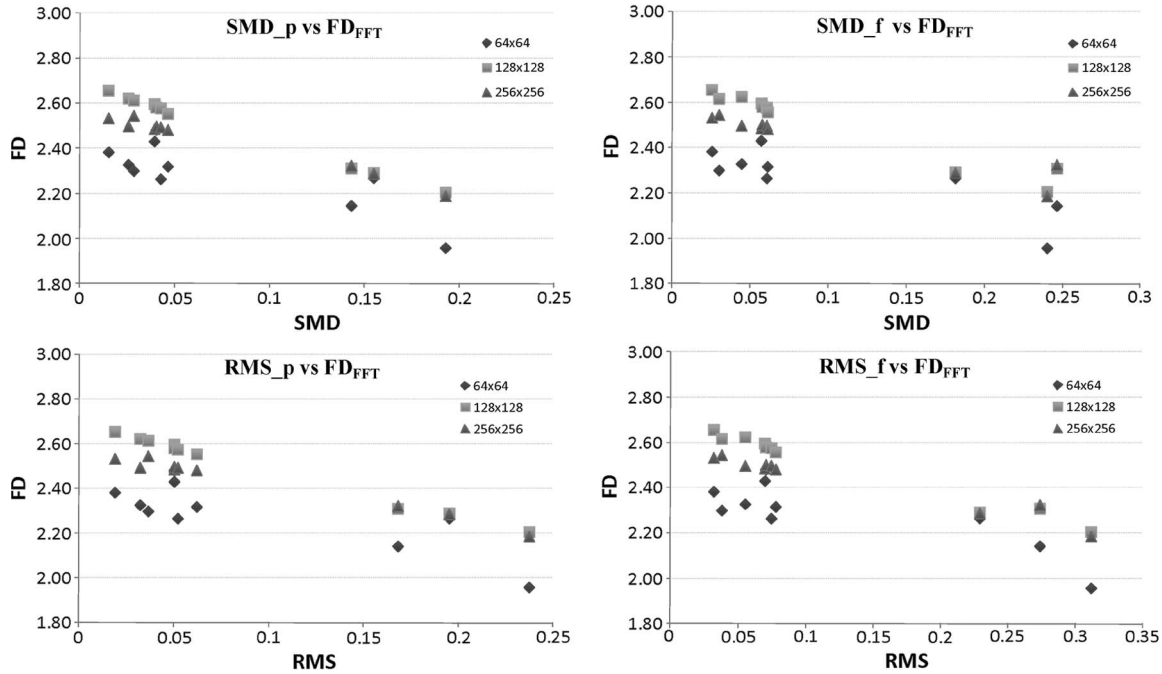

Fig. 18. Comparison of FD_{FFT} and standard roughness parameters. "_p" refers to the second-order polynomial surface, and "_f" refers to the flat plane.

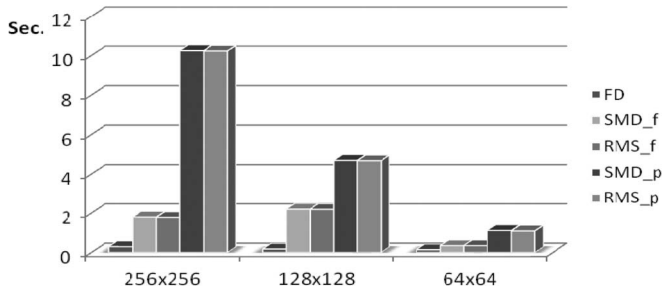

Fig. 19. Comparison of the computation time.

data, the Pearson's correlation coefficients are around 0.82. The results demonstrated that FD_{FFT} was highly related to SMD and RMS. Moreover, the computation of FD_{FFT} is much faster than the computation of the standard roughness parameters. We can conclude that FD_{FFT} is a fast reliable parameter for evaluating fabric surface roughness.

V. Conclusion

This paper has discussed new computer vision and 3-D image analysis techniques for a fast, accurate, noncontact, and nondestructive automatic texture analysis of woven fabric.

In Section II, we proposed a method that allows automatic recognition of basic weave pattern and precisely measuring the yarn count. The yarn crossed areas are segmented by a spatial domain integral projection approach. By combining FCM and PCA on GLCM feature vectors extracted from the segments, we can classify the detected segments into two clusters. Based on the analysis on texture orientation features, the yarn crossed-area states are automatically determined. An autocorrelation method is used to find weave repeats and correct detection errors. The method was validated by using computer-simulated woven samples and real woven fabric images. The test samples have various yarn counts, appearance, and weave types. All weave patterns of the tested fabric samples are successfully recognized, and computed yarn counts are consistent with the manual counts. In Section III, we proposed a 2DFFT-based fractal dimension parameter FD_{FFT} to characterize the surface roughness of fabrics from 3-D fabric images. Its robustness to image rotations and scaling was validated with fractal Brownian images. The standard roughness parameters SMD and RMS were used to test the validity of FD_{FFT} as a reliable parameter for fabric roughness characterization. Tests have shown that FD_{FFT} values are highly correlated with the standard roughness parameters.

Acknowledgment

The authors would like to thank XYZ RGB Inc. for providing help with the 3-D laser scan of their fabric samples.

References

[1] S. Kawabata, *The Standardization and Analysis of Hand Evaluation,* 2nd ed. Osaka, Japan: Hand Eval. Standardization Committee, Textile Mach. Soc. Jpn., 1980.

[2] S. Moslehpour, C. Campana, D. Shetty, and B. Deryniosky, "Stand-alone surface roughness analyzer," *IEEE Trans. Instrum. Meas.*, vol. 58, no. 3, pp. 698–706, Mar. 2009.

[3] A. W. Domanski and T. R. Wolinski, "Surface roughness measurement with optical fibers," *IEEE Trans. Instrum. Meas.*, vol. 41, no. 6, pp. 1057–1061, Dec. 1992.

[4] K. Zhang, C. Butler, Q. Yang, and Y. Lu, "A fiber optic sensor for the measurement of surface roughness and displacement using artificial neural networks," *IEEE Trans. Instrum. Meas.*, vol. 46, no. 4, pp. 899–902, Aug. 1997.

[5] G. P. P. Gunarathne and K. Christidis, "Measurements of surface texture using ultrasound," *IEEE Trans. Instrum. Meas.*, vol. 50, no. 5, pp. 1144–1148, Oct. 2001.

[6] J. Scharcanski, "Stochastic texture analysis for measuring sheet formation variability in the industry," *IEEE Trans. Instrum. Meas.*, vol. 55, no. 5, pp. 1778–1785, Oct. 2006.

[7] J. Scharcanski and C. T. J. Dodson, "Stochastic texture image estimators for local spatial anisotropy and its variability," *IEEE Trans. Instrum. Meas.*, vol. 49, no. 5, pp. 971–979, Oct. 2000.

[8] A. Abouelela, H. M. Abbas, H. Eldeeb, A. A. Wahdan, and S. M. Nassar, "Automatic vision system for localizing structural defects in textile fabrics," *Pattern Recognit. Lett.*, vol. 26, no. 10, pp. 1435–1443, Jul. 2005.
[9] J. G. Campbell and F. Murtagh, "Automatic visual inspection of woven textiles using a two-stage defect detector," *Opt. Eng.*, vol. 37, no. 9, pp. 2536–2542, Sep. 1998.
[10] N. M. Botros, "A PC-based tissue classification system using artificial neural networks," *IEEE Trans. Instrum. Meas.*, vol. 41, no. 5, pp. 633–638, Oct. 1992.
[11] S. Osowski, R. Siroic, T. Markiewicz, and K. Siwek, "Application of support vector machine and genetic algorithm for improved blood cell recognition," *IEEE Trans. Instrum. Meas.*, vol. 58, no. 7, pp. 2159–2168, Jul. 2009.
[12] S. Xiong and Z. Zhou, "A complex nonlinear exponential autoregressive model approach to shape recognition using neural networks," *IEEE Trans. Instrum. Meas.*, vol. 49, no. 6, pp. 1298–1304, Dec. 2000.
[13] S. Chakravarthy, R. Sharma, and R. Kasturi, "Noncontact level sensing technique using computer vision," *IEEE Trans. Instrum. Meas.*, vol. 51, no. 2, pp. 353–361, Apr. 2002.
[14] L. V. Fausett, *Applied Numerical Analysis Using Matlab*. Englewood Cliffs, NJ: Prentice-Hall, 1999.
[15] B. S. Jeon, J. H. Bae, and M. W. Suh, "Automatic recognition of woven fabric patterns by an artificial neural network," *Textile Res. J.*, vol. 73, no. 7, pp. 645–650, Jul. 2003.
[16] C. F. J. Kuo, C. Y. Shih, and J. Y. Lee, "Automatic recognition of fabric weave patterns by a fuzzy C-means clustering method," *Textile Res. J.*, vol. 74, no. 2, pp. 107–111, Feb. 2004.
[17] B. G. Xu, "Identifying fabric structures with Fast Fourier Transform techniques," *Textile Res. J.*, vol. 66, no. 8, pp. 496–506, Aug. 1996.
[18] M. Kinoshita, Y. Hashimoto, R. Akiyama, and S. Uchiyama, "Determination of weave type in woven fabric by digital image processing," *J. Textile Mach. Soc. Jpn.*, vol. 35, no. 2, pp. 1–4, 1989.
[19] A. Lachkar, T. Gadi, R. Benslimane, and L. D'Orazio, "Textile woven fabric recognition using Fourier image analysis techniques: Part I: A fully automatic approach for crossed-points detection," *J. Textile Inst.*, vol. 94, no. 3/4, pp. 194–201, 2003.
[20] A. Lachkar, R. Benslimane, L. D'Orazio, and E. Martuscelli, "Textile woven fabric recognition using Fourier image analysis techniques: Part II—Texture analysis for crossed-states detection," *J. Textile Inst.*, vol. 96, no. 3, pp. 179–183, Jun. 2005.
[21] C. F. J. Kuo, C. Y. Shih, and J. Y. Lee, "Repeat pattern segmentation of printed fabrics by Hough transform method," *Textile Res. J.*, vol. 75, no. 11, pp. 779–783, Nov. 2005.
[22] T. J. Kang, C. H. Kim, and K. W. Oh, "Automatic recognition of fabric weave patterns by digital image analysis," *Textile Res. J.*, vol. 69, no. 2, pp. 77–83, Feb. 1999.
[23] C. F. J. Kuo and C. C. Tsai, "Automatic recognition of fabric nature by using the approach of texture analysis," *Textile Res. J.*, vol. 76, no. 5, pp. 375–382, May 2006.
[24] M. Rallo, J. Escofet, and M. S. Millan, "Weave-repeat identification by structural analysis of fabric images," *Appl. Opt.*, vol. 42, no. 17, pp. 3361–3372, Jun. 2003.
[25] X. Wang, N. D. Georganas, and E. M. Petriu, "Fiber-level structure recognition of woven textile," in *Proc. IEEE Int. Workshop HAVE*, Lecco, Italy, Nov. 2009, pp. 117–122.
[26] R. M. Haralick, K. Shanmugam, and I. Dinstein, "Textural features for image classification," *IEEE Trans. Syst., Man, Cybern.*, vol. SMC-3, no. 6, pp. 610–621, Nov. 1973.
[27] I. T. Jolliffe, *Principal Component Analysis,* 2nd ed. New York: Springer-Verlag, 2002.
[28] E. Anderson, Z. Bai, C. Bischof, S. Blackford, J. Demmel, J. Dongarra, J. Du Croz, A. Greenbaum, S. Hammarling, A. McKenney, and D. Sorensen, *LAPACK User's Guide,* 3rd ed. Philadelphia, PA: SIAM, 1999.
[29] W. Chumsamrong, P. Thitimajshima, and Y. Rangsanseri, "Synthetic aperture radar (SAR) image segmentation using a new modified fuzzy c-means algorithm," in *Proc. Geosci. Remote Sens. Symp.*, 2000, vol. 2, pp. 624–626.
[30] P. Palisson, N. Zegadi, F. Peyrin, and R. Unterreiner, "Unsupervised multiresolution texture segmentation using wavelet decomposition," in *Proc. 1st IEEE Int. Conf. Image Process.*, Austin, TX, Nov. 1994, pp. 625–629.
[31] H. Sari-Sarraf and J. S. Goddard, Jr., "Online optical measurement and monitoring of yarn density in woven fabrics," *Proc. SPIE*, vol. 2899, pp. 444–452, 1996.
[32] T. J. Kang, S. C. Kim, I. H. Sul, J. R. Youn, and K. Chung, "Fabric surface roughness evaluation using wavelet-fractal method: Part I—Wrinkle, smoothness and seam pucker," *Textile Res. J.*, vol. 75, no. 11, pp. 751–760, Nov. 2005.
[33] X. Wang and N. D. Georganas, "GLCM texture based fractal method for evaluating fabric surface roughness," in *Proc. IEEE CCECE*, May 2009, pp. 104–107.
[34] R. Zwiggelaar and C. R. Bull, "Optical determination of fractal dimensions using Fourier transforms," *Opt. Eng.*, vol. 34, no. 5, pp. 1325–1332, May 1995.

Xin Wang received the B.A.Sc. (*summa cum laude*) and M.A.Sc. degrees in electrical engineering in 2004 and 2006, respectively, from the University of Ottawa, Ottawa, ON, Canada, where she is currently working toward the Ph.D. degree in electrical and computer engineering.

Her research interests include image processing, pattern recognition, texture classification, computer graphics, and fabric structure modeling.

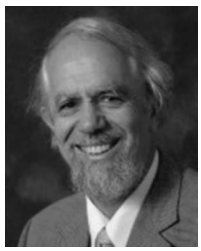

Nicolas D. Georganas (F'90–LF'09) received the Dipl.Ing. degree in electrical and mechanical engineering from the National Technical University of Athens (NTUA), Athens, Greece, in 1966, the Ph.D. degree (*summa cum laude*) in electrical engineering from the University of Ottawa, Ottawa, ON, Canada, in 1970, the Honorary Ph.D. degree from the Technical University Darmstadt, Darmstadt, Germany, in 2004, and the Honorary Ph.D. degree from NTUA in 2007.

He is currently a Distinguished University Professor with the School of Information Technology and Engineering, University of Ottawa. He has authored more than 360 technical papers and coauthored the book *Queueing Networks—Exact Computational Algorithms: A Unified Theory by Decomposition and Aggregation* (Cambridge, MA: MIT Press, 1989). His research interests include multimedia communications, collaborative virtual environments, Web telecollaboration applications, intelligent Internet sensors and appliances, and telehaptics.

Dr. Georganas is a Fellow of the Engineering Institute of Canada, the Canadian Academy of Engineering, and the Royal Society of Canada. In 2004, he became the Founding Editor-in-Chief of the *ACM Transactions on Multimedia Computing, Communications and Applications*. In 2005, he was recognized as a Pioneer of Computing in Canada by the International Business Machines Corporation Centre of Advanced Studies. In 2007, he was invested Officer of the Order of Canada (the highest honor for a Canadian). He was the recipient of the Killam Prize for Engineering in 2002, the Queens Golden Jubilee Medal in 2003, the Canadian Award in Telecommunications Research in 2006, the first IEEE Canada Computer Medal, and the ORION Leadership Award.

Emil M. Petriu (M'86–SM'88–F'01) received the Dipl.Eng. and Dr. Eng. degrees from the Polytechnic Institute of Timisoara, Timisoara, Romania, in 1969 and 1978, respectively.

He is currently a Professor and a University Research Chair with the School of Information Technology and Engineering, University of Ottawa, Ottawa, ON, Canada. During his career, he has published more than 200 technical papers, authored two books, and edited two other books. He is the holder of two patents. His research interests include robot sensing and perception, intelligent sensors, interactive virtual environments, soft computing, and digital integrated circuit testing.

Dr. Petriu is a Fellow of the Canadian Academy of Engineering and of the Engineering Institute of Canada. He is an Associate Editor of the IEEE TRANSACTIONS ON INSTRUMENTATION AND MEASUREMENT and a member of the Editorial Board of the IEEE I&M MAGAZINE. He is currently the Chair of TC-15 Virtual Systems and the Cochair of TC-28 Instrumentation and Measurement for Robotics and Automation and TC-30 Security and Contraband Detection of the IEEE Instrumentation and Measurement Society. He was a corecipient of the IEEE's Donald G. Fink Prize Paper Award and the recipient of the IEEE Instrumentation and Measurement Society Award in 2003.